

## Stress regime in the Philippine Sea slab beneath Kanto, Japan

Junichi Nakajima,<sup>1</sup> Akira Hasegawa,<sup>1</sup> and Fuyuki Hirose<sup>2</sup>

Received 3 July 2011; accepted 24 July 2011; published 31 August 2011.

[1] We determine the focal mechanisms of earthquakes within the Philippine Sea slab beneath the Tokyo metropolitan area, and perform stress tensor inversions to investigate the detailed stress field within the slab. The results show a characteristic spatial variation in earthquake-generating stress. Slab stress in northeastern part of the PHS slab is characterized by down-dip tension (DDT), except for the uppermost tip of the seismic portion of the slab where down-dip compression (DDC) stress is dominant. We interpret that DDT is caused by the net slab pull and DDC is attributable to local resistance to subduction at the tip of the slab. In southwestern part of the PHS slab,  $\sigma_1$  and  $\sigma_3$  are generally rotated oblique to the dip of the slab, suggesting that earthquakes occur under stress conditions of neither DDC nor DDT. The rotations in  $\sigma_1$  and  $\sigma_3$  may be related to stress accumulation by the slip deficit along the asperity of the 1923 Kanto earthquake (M7.9). **Citation:** Nakajima, J., A. Hasegawa, and F. Hirose (2011), Stress regime in the Philippine Sea slab beneath Kanto, Japan, *Geophys. Res. Lett.*, 38, L16318, doi:10.1029/2011GL048754.

### 1. Introduction

[2] The Kanto district is located in a unique tectonic setting, characterized by the subduction of two oceanic plates, the Philippine Sea (PHS) and Pacific (PAC) plates. The PHS plate is subducting beneath the North American (NA) plate, and the PAC plate is subducting beneath both the NA and PHS plates [e.g., Seno *et al.*, 1993] (Figure 1). As a result of this dual plate subduction, many M ~ 8 and numerous M ~ 7 earthquakes have repeatedly struck Tokyo, such as the 1923 Kanto earthquake (M7.9) that occurred along the upper surface of the PHS plate. *Central Disaster Management Council* [2004] has estimated ~11,000 fatalities and economic losses of up to 112 trillion yen if an earthquake (M7.3) occurs along the PHS slab in the northern part of Tokyo bay.

[3] The seismic activity of small earthquakes beneath Kanto has been discussed in terms of the thick (~60 km) PHS slab, and frictional and mechanical interactions along the PHS-PAC slab contact zone [e.g., Wu *et al.*, 2007; Nakajima *et al.*, 2009; Uchida *et al.*, 2009]. Focal mechanisms of earthquakes in the PHS slab show that stress regimes of down-dip compression (DDC) and down-dip tension (DDT) are dominant in the upper and lower parts of the slab, respectively [Hori, 2006]. These focal mechanisms are different from those observed in the PHS slab beneath south-

western Japan [e.g., Wang *et al.*, 2004], indicating that the slab stress beneath Kanto is influenced by the local slab geometry or other factors. However, the great diversity of seismic activity and the complex geometry of the slab have prevented systematic investigations of the stress field within the PHS slab.

[4] This study discriminates earthquakes within the PHS slab from other earthquakes based on the recently determined geometries of the PHS and PAC slabs [Hirose *et al.*, 2008; Nakajima *et al.*, 2009], and investigates the stress regime in the PHS slab in detail. The resulting spatial variations in the stress regime are discussed in terms of bending/unbending of the slab, negative buoyancy of the slab, resistance to slab subduction, and stress accumulated by a locked portion of the 1923 Kanto earthquake asperity.

### 2. Focal Mechanism Solutions

[5] The Japan Meteorological Agency (JMA) routinely determines focal mechanism solutions of earthquakes with  $M \geq 3.2$  beneath the Japanese Islands. To increase the amount of focal mechanism data, we determined focal mechanism solutions of smaller earthquakes by reading the initial P-wave polarities from raw records. First, we relocated earthquakes ( $M < 3.2$ ) in the JMA catalogue beneath Kanto for the period from March 2001 to July 2010 using the 3D P- and S-wave velocity structures obtained by Nakajima and Hasegawa [2010]. Then, earthquakes that occurred within the PHS slab were selected based on the geometries of the PHS and PAC slabs [Hirose *et al.*, 2008; Nakajima *et al.*, 2009]. P-wave polarities were manually picked by careful inspection of the data recorded at stations shown in Figure S1 in auxiliary material, and focal mechanism solutions were determined for earthquakes with 10 or more polarity data, using the method of Hardebeck and Shearer [2002].<sup>1</sup> To ensure well-constrained solutions, we only considered focal mechanism solutions with polarity errors of <10% and high quality (Quality A and B). Finally, we removed interplate earthquakes of the PHS and PAC slabs that satisfy both of the following criteria: (1) earthquakes with low-angle thrust-type focal mechanisms and with a slip vector consistent with the relative motion of each plate, and (2) earthquakes within <10 km from the upper surface of each of the PHS or PAC slabs. As a result, we obtained highly-accurate focal mechanism solutions for 79 earthquakes, 53 of which have  $M \leq 2.5$  (Figure S2). We also consider the JMA-determined focal mechanism solutions of 165 earthquakes within the PHS slab. The focal mechanism solutions of the 244 earthquakes are shown in Figure S3.

[6] The obtained orientations of P and T axes are shown in Figures 2b, 2c, 3a, and 3b. Earthquakes in northeast Kanto

<sup>1</sup>Research Center for Prediction of Earthquakes and Volcanic Eruptions, Graduate School of Science, Tohoku University, Sendai, Japan.

<sup>2</sup>Seismology and Volcanology Research Department, Meteorological Research Institute, Tsukuba, Japan.

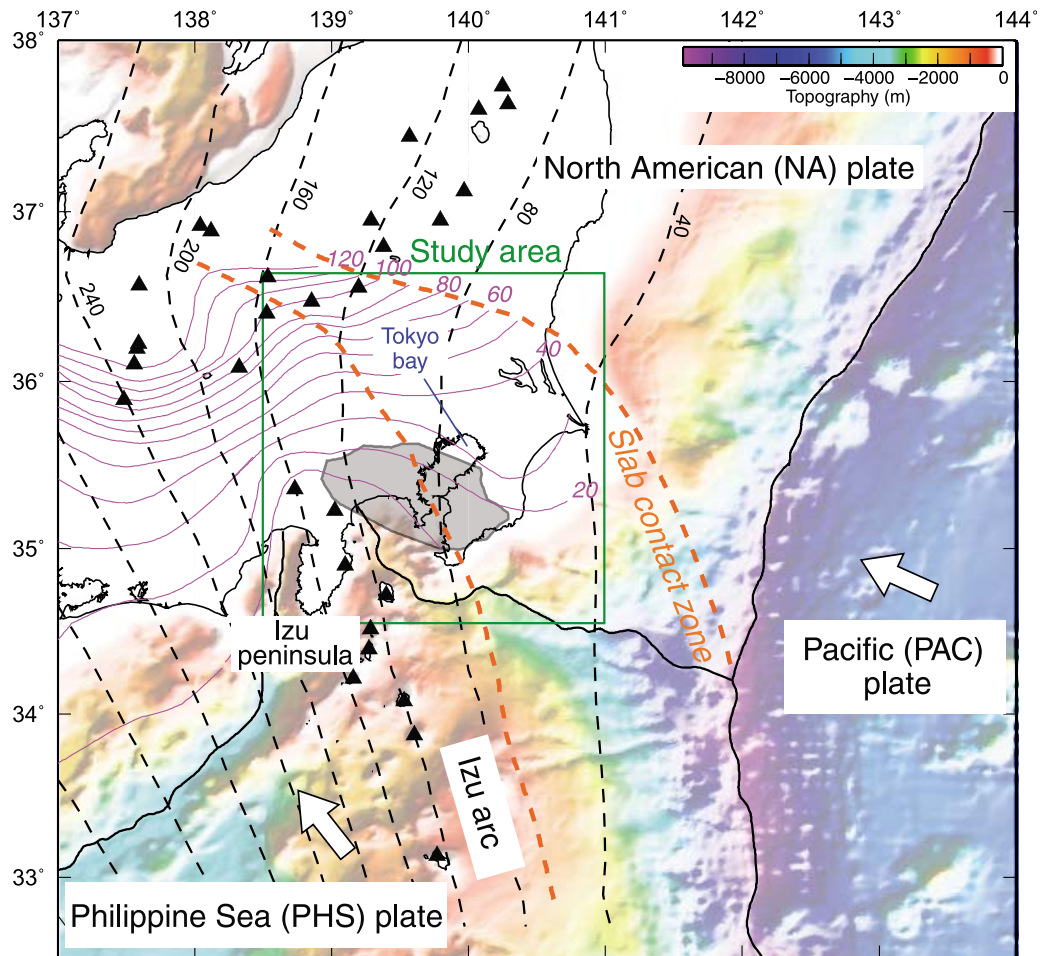


**Figure 1.** Tectonic setting of the central part of Japan. Black dashed and pink contours denote the upper surfaces of the Pacific (PAC) and Philippine Sea (PHS) plates, respectively [Hirose *et al.*, 2008; Nakajima *et al.*, 2009], and orange dashed lines denote the PHS-PAC contact zone [Uchida *et al.*, 2009]. Arrows indicate the directions of motion of the PHS and PAC plates relative to the North American plate [e.g., Seno *et al.*, 1993]. Black triangles denote active volcanoes. The gray region indicates the slip area of the 1923 Kanto earthquake (M7.9) [Wald and Somerville, 1995]. Seafloor topography is shown by color shading.

generally have T axes oriented in the down-dip direction (lines A–D in Figure 3). The exception is earthquakes that occurred at the northwestern tip of the seismic portion of the PHS slab, where down-dip P axes are dominant in the uppermost part of the slab. In contrast to lines A–D, focal mechanisms for earthquakes in southwest Kanto (lines E and F) show that the dip angles of P and T axes are oblique to the dip of the slab in the middle part of the PHS slab. Earthquakes in the lowermost part of the PHS slab have characteristic focal mechanisms, with P axes oriented parallel to the upper surface of the underlying PAC slab (lines D and E in Figure 3).

### 3. Stress Tensor Inversions

[7] To investigate the regional stress field in the PHS slab, we applied the stress tensor inversion method of Ito *et al.* [2009] to the obtained focal mechanism data. For the calculation, we set 280 grid nodes within the PHS slab with horizontal and vertical intervals of 20 km and 10 km, respectively, and performed stress tensor inversions using the 15 nearest earthquakes from each grid node. If 15 earthquakes were not

located within a radius of 25 km from a given grid node, the node was not involved in the inversion. As a result, we obtained inversion results for 96 nodes (Figure S4). It is noted that we obtained almost the same results when we used different grid intervals, number of earthquakes, and radius in the inversions.

[8] The orientations of  $\sigma_1$  and  $\sigma_3$  for each node are shown in Figures 2d and 3c. The results show clear spatial variations in the orientations of  $\sigma_1$  and  $\sigma_3$ . The orientation of  $\sigma_3$  is generally down-dip along lines A–D, suggesting that DDT stress is dominant in the PHS slab. However, DDC stress is observed locally in the upper part of the slab (horizontal axis, X, of  $\geq 120$  km in lines C and D in Figure 3c). In southwest Kanto,  $\sigma_1$  is generally oriented in the direction of relative plate motion (Figure 2d). However, the dips of  $\sigma_1$  and  $\sigma_3$  are oblique to the dip of the slab ( $60 \text{ km} \leq X \leq 100 \text{ km}$  in lines E and F), resulting in rotations of  $\sigma_1$  and  $\sigma_3$  compared with their orientations in lines A–D. Consequently, earthquakes in these areas occur under stress conditions of neither DDC nor DDT. The rotations of  $\sigma_1$  and  $\sigma_3$  appear to occur beneath the asperity of the 1923 Kanto earthquake (M7.9). It is noted that earthquakes in the uppermost part of the slab

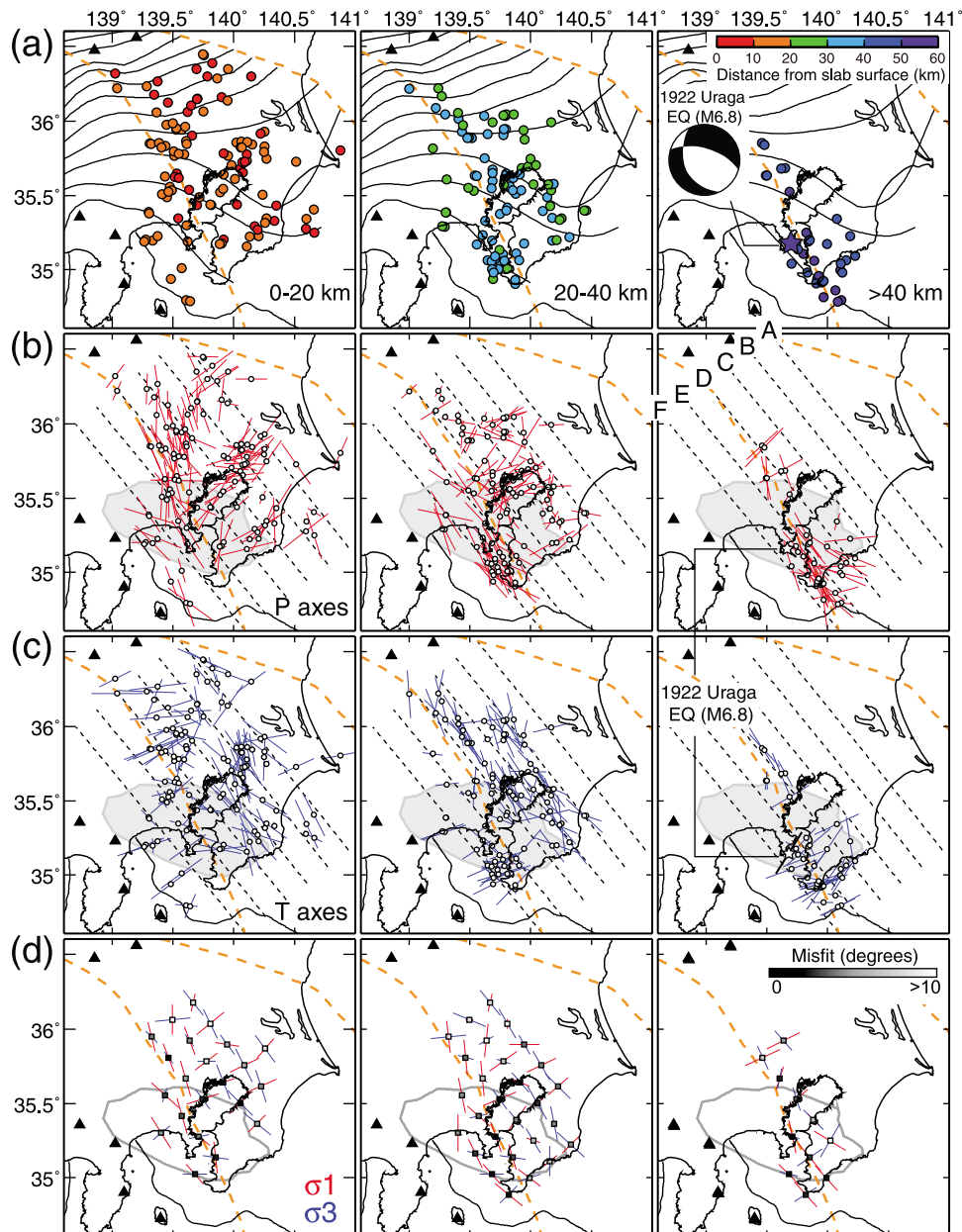


**Figure 2.** Distributions of (a) hypocenters, (b) P and (c) T axes for earthquakes that occurred in the PHS slab in the distance range of (left) 0–20 km, (middle) 20–40 km, and (right) >40 km from the upper slab surface. Colors in Figure 2a denote the distance from the slab surface. Dashed lines A–F in Figure 2b (right) indicate the locations of cross sections shown in Figures 3 and 4. The hypocenter of the 1922 Uruga channel earthquake (M6.8) (star) and its focal mechanism solution [Ishibashi, 1975b] are shown in Figure 2a (right). (d) Orientations of the best-fit  $\sigma_1$  (red) and  $\sigma_3$  (blue) obtained by stress tensor inversions. The location of each grid node is shown by a square. Gray scales in squares indicate the value of misfit calculated in the inversions. Other symbols are the same as in Figure 1.

still occur under DDC stress, even in southwest Kanto ( $X \geq 100$  km in lines E and F).

#### 4. Discussion and Conclusions

[9] Slab bending/unbending stress has been invoked as the cause of DDC and DDT stresses in a subducting slab [e.g., Engdahl and Scholz, 1977]. Based on a 2D plate model, the magnitude of unbending stress is estimated to be on the order of 100 MPa [e.g., Tsukahara, 1980]. However, a quantitative estimation is difficult in the case of a com-

plicated slab geometry. Instead, we calculated the changes in the curvature of the upper surface of the PHS plate with respect to the subduction direction, because an increase or decrease in curvature can result in the generation of the DDT or DDC stresses, respectively, in the uppermost part of the slab. Squares with colors ranging from red to blue in Figure 3c shows the stress field immediately below the upper surface of the PHS slab, as predicted from the slab geometry. The predicted stress regime is DDT for all lines at  $X \geq 100$  km. However, the observed stress regime is clearly DDC for the corresponding areas along lines C–F. Deformation due to

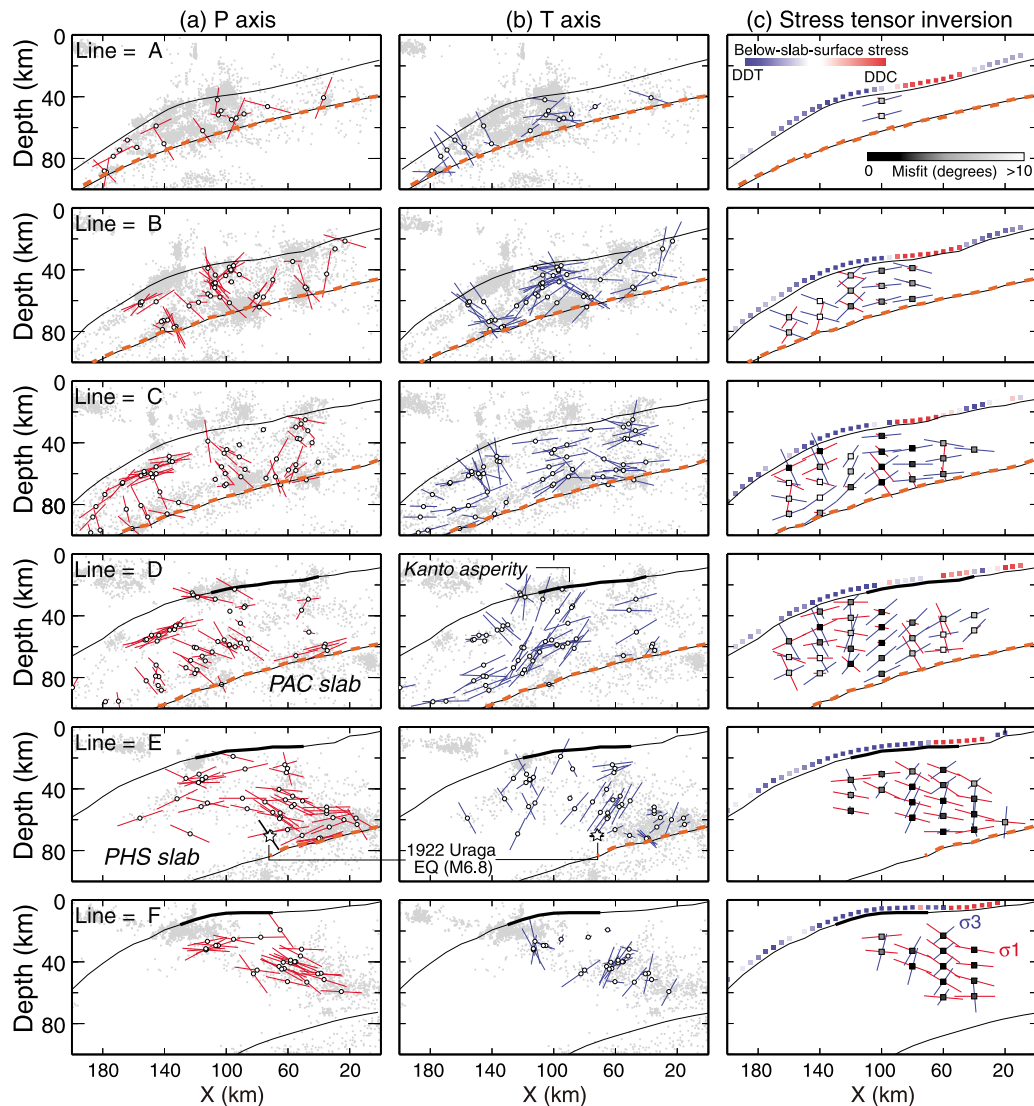


**Figure 3.** Cross sections showing the orientations of (a) P and (b) T axes along lines A–F in Figure 2, together with background seismicity (gray circles). Black curves denote the upper surfaces of the PHS and PAC slabs. Thick black and dashed orange curves indicate the asperity of the 1923 Kanto earthquake and the PHS-PAC contact zone, respectively. The orientations of P and T axes of the 1922 Uruga channel earthquake (M6.8) [Ishibashi, 1975b] are shown by black bars in line E. (c) Cross sections showing the orientations of  $\sigma_1$  (red) and  $\sigma_3$  (blue) obtained by stress tensor inversions. Gray scales in squares indicate the value of misfit calculated in the inversions. The stress regime in the uppermost part of the PHS slab, as predicted from the slab geometry, is shown by squares with colors ranging from red (DDC) to blue (DDT) along the top of the slab surface (see the text for details).

bending/unbending cannot account for the observed stress regime, at least in the uppermost part of the slab, and hence may not be a dominant factor on controlling the stress in the PHS slab.

[10] The net slab pull, which corresponds to negative buoyancy minus resistive drag exerted by the mantle on the slab, is considered to be about 10% [Schellart, 2004] or 70–100% [Conrad and Lithgow-Bertelloni, 2002] of the total negative buoyancy of the slab. We calculated an approximate value of the negative buoyancy for a simplified geometry of the PHS slab beneath Kanto (thickness: 50 km, length: 150 km, width: 200 km), using the equation of Turcotte and Schubert [2002], and obtained the slab pull to be  $\sim 40$  MPa. The net slab pull is then estimated to be 4–40 MPa. This net slab pull generates the tensional stress

inherent in the slab, and explains the DDT stress observed along lines A–D.

[11] The unique tectonic setting around Kanto has given rise to two types of resistances in the PHS plate. One is resistance due to accretion of the shallower portion of the buoyant PHS plate onto the NA plate at the north of the Izu peninsula [e.g., Tamura et al., 2010]. This resistance can act efficiently on both sides of the peninsula, generating compressional stress in the PHS plate. The other is resistance resulting from subduction of the PHS plate into the confined space between the overlying NA and underlying PAC plates [e.g., Wu et al., 2007], which may result in compressional stress at the tip of the PHS plate [e.g., Hori, 2006]. We consider that large compressional stress, even though it is difficult to estimate its magnitude, has locally become dom-

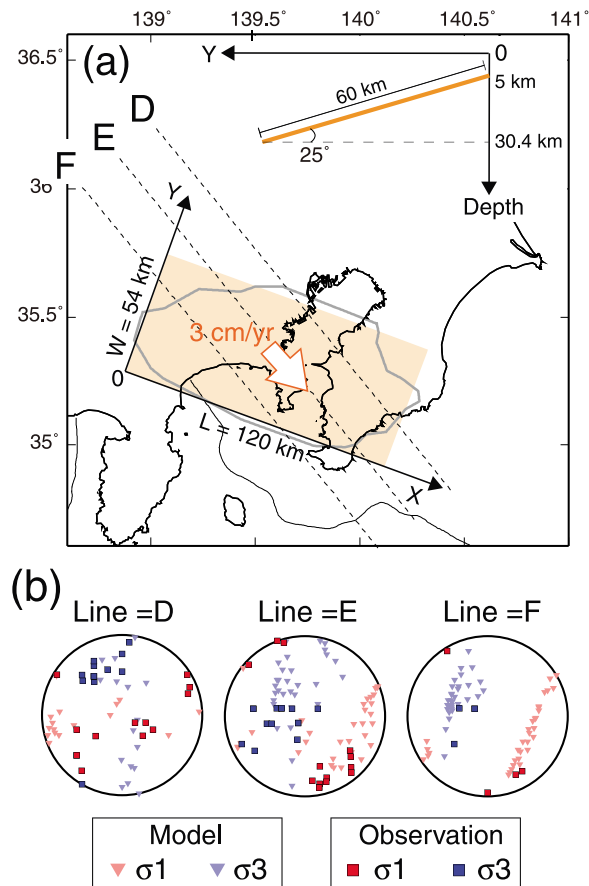


**Figure 4.** (a) The extent of the fault model (orange rectangle) used for calculating the stress field caused by the slip deficit of the Kanto asperity. The area outlined by gray denotes the slip area of the 1923 Kanto earthquake [Wald and Somerville, 1995]. The white arrow shows the direction of slip along the fault. The insert shows a cross section of the fault model (orange line). (b) Equal-area polar plots of calculated (reverse triangles) and observed (squares)  $\sigma_1$  and  $\sigma_3$  for grid nodes located beneath the Kanto asperity along lines D–F in Figure 4a.

inant over the inherent tensional stress, thereby generating the DDC stress regime only at the tip of the seismic portion of the PHS slab ( $X \geq 120$  km in lines C and D and  $X \geq 100$  km in lines E and F in Figure 3c).

[12] To explain the rotations of  $\sigma_1$  and  $\sigma_3$  observed in southwest Kanto, we evaluated the stress field associated with interplate coupling along the asperity of the 1923 Kanto earthquake (M7.9), using the back-slip model [Savage, 1983]. A normal-fault-type movement is introduced along the Kanto asperity to model the occurrence of interplate coupling, and the principal stress is calculated for a medium with a Poisson's ratio of 0.25, using the method of Okada [1992]. The geometry and location of the asperity and the slip direction (N138°E) are taken from Wald and Somerville [1995], considering a slip rate of 3 cm/yr [e.g., Seno et al., 1993] (Figure 4a).

[13] The calculated results show that  $\sigma_1$  and  $\sigma_3$  beneath the asperity are oriented oblique to the dip of the slab surface (Figures 4b and S5). Along lines E and F, the orientations of observed  $\sigma_1$  and  $\sigma_3$  are consistent approximately with those

derived from the model, although the modeled  $\sigma_1$  tends to be oriented more eastward than the observations (Figure 4b). These results suggest that the observed stress regime is partly affected by the stress accumulated by the slip deficit of the Kanto asperity. The problem here is that an average value of stress accumulation beneath the asperity is  $\sim 17$  KPa for the slip deficit of 3 cm/yr. Therefore, the amount of stress accumulation over 88 years since 1923 is  $\sim 1.5$  MPa, which is insufficient enough to overcome the tensional stress inherent in the PHS slab (4–40 MPa). However, in the case that subduction of the buoyant Izu volcanic arc in the area south of the asperity (Figure 1) can result in a marked reduction in the net slab pull, the stress accumulated by interplate coupling would have a dominant effect locally on the stress field. The discrepancy in the orientations of  $\sigma_1$  and  $\sigma_3$  between the model and observations for line D (Figure 4b) suggests that the magnitude of the net slab pull is no longer sufficiently small to reflect the stress disturbed by interplate coupling.

[14] Ishibashi [1975a] relocated the hypocenter of the 1922 Uraga channel earthquake (M6.8), one of the largest earthquakes beneath Tokyo, in the PHS slab (white stars in Figures 2 and 3). However, uncertainties in the hypocentral location were relatively large, with horizontal and vertical errors of  $\pm 25$  km and  $\pm 21$  km, respectively. Considering the orientation of P axis (line E in Figure 3), which is more reliably constrained than those of the other axes [Ishibashi, 1975b], the Uraga event is likely to be located slightly southeastward ( $X = 50$ – $60$  km) and at depths of 50–60 km. The Uraga event may have occurred before the 1923 Kanto earthquake in an area where the stress field is affected by the slip deficit of the Kanto asperity, although this interpretation needs to be confirmed by further investigations of the focal mechanism of the Uraga event based on the precise location of the hypocenter.

[15] **Acknowledgments.** The authors would like to thank Y. Ito, T. Iinuma and Y. Ohta for fruitful discussion. Constructive and careful reviews by two anonymous reviewers improved the paper significantly. We used focal mechanism solutions listed in the unified catalogue of the JMA. All the figures in this paper are plotted by Generic Mapping Tools [Wessel and Smith, 1998]. This work was supported in part by the Ministry of Education, Culture, Sports, Science and Technology of Japan, under its Observation and Research Program for Prediction of Earthquakes and Volcanic Eruptions.

[16] The Editor thanks two anonymous reviewers for their assistance in evaluating this paper.

## References

- Central Disaster Management Council (2004), Report of the 12th Special Committee on the Earthquake just beneath the Tokyo Metropolis [in Japanese], Gov. of Jpn., Tokyo. [Available at <http://www.bousai.go.jp/jishin/chubou/shutochokka/12/index.html>.]
- Conrad, C. P., and C. Lithgow-Bertelloni (2002), How mantle slabs drive plate tectonics, *Science*, *298*, 207–209, doi:10.1126/science.1074161.
- Engdahl, E. R., and C. H. Scholz (1977), A double Benioff zone beneath the central Aleutians: An unbending of the lithosphere, *Geophys. Res. Lett.*, *4*, 473–476, doi:10.1029/GL004i010p00473.
- Hardebeck, J. L., and P. M. Shearer (2002), A new method for determining first-motion focal mechanisms, *Bull. Seismol. Soc. Am.*, *92*, 2264–2276, doi:10.1785/0120010200.
- Hirose, F., J. Nakajima, and A. Hasegawa (2008), Three-dimensional velocity structure and configuration of the Philippine Sea slab beneath Kanto district, central Japan, estimated by double-difference tomography [in Japanese with English abstract], *J. Seismol. Soc. Jpn.*, *60*, 123–138.
- Hori, S. (2006), Seismic activity associated with the subducting motion of the Philippine Sea plate beneath the Kanto district, Japan, *Tectonophysics*, *417*, 85–100, doi:10.1016/j.tecto.2005.08.027.

- Ishibashi, K. (1975a), Precise relocation of semi-historical earthquakes using S-P times under a multi-layered structure model [in Japanese with English abstract], *J. Seismol. Soc. Jpn.*, *28*, 347–364.
- Ishibashi, K. (1975b), Earthquake-generation stress before the 1923 Kanto earthquake beneath the Kanto district: An indicator of the occurrence of megathrust earthquake along the Sagami trough [in Japanese], paper presented at Fall Meeting, Seismol. Soc. of Jpn., Tsukuba.
- Ito, Y., Y. Asano, and K. Obara (2009), Very-low-frequency earthquakes indicate a transpressional stress regime in the Nankai accretionary prism, *Geophys. Res. Lett.*, *36*, L20309, doi:10.1029/2009GL039332.
- Nakajima, J., and A. Hasegawa (2010), Cause of  $M \sim 7$  intraslab earthquakes beneath the Tokyo metropolitan area: Possible evidence for a vertical slab tear at the easternmost portion of the Philippine Sea slab, *J. Geophys. Res.*, *115*, B04301, doi:10.1029/2009JB006863.
- Nakajima, J., F. Hirose, and A. Hasegawa (2009), Seismotectonics beneath the Tokyo Metropolitan area, Japan: Effect of slab-slab contact and overlap on seismicity, *J. Geophys. Res.*, *114*, B08309, doi:10.1029/2008JB006101.
- Okada, Y. (1992), Internal deformation due to shear and tensile faults in a half space, *Bull. Seismol. Soc. Am.*, *82*, 1018–1040.
- Savage, J. C. (1983), A dislocation model of strain accumulation and release at a subduction zone, *J. Geophys. Res.*, *88*, 4984–4996, doi:10.1029/JB088iB06p04984.
- Schellart, W. P. (2004), Quantifying the net slab pull force as a driving mechanism for plate tectonics, *Geophys. Res. Lett.*, *31*, L07611, doi:10.1029/2004GL019528.
- Seno, T., S. Stein, and A. E. Gripp (1993), A model for the motion of the Philippine Sea plate consistent with NUVEL-1 and geological data, *J. Geophys. Res.*, *98*, 17,941–17,948, doi:10.1029/93JB00782.
- Tamura, Y., et al. (2010), Missing Oligocene crust of the Izu-Bonin arc: Consumed or rejuvenated during collision?, *J. Petrol.*, *51*, 823–846, doi:10.1093/ptrology/egg002.
- Tsukahara, H. (1980), Physical conditions for double-seismic planes of the deep seismic zone, *J. Phys. Earth*, *28*, 1–15, doi:10.4294/jpe1952.28.1.
- Turcotte, D. L., and G. Schubert (2002), *Geodynamics*, 2nd ed., 458 pp., Cambridge Univ. Press., New York.
- Uchida, N., J. Nakajima, A. Hasegawa, and T. Matsuzawa (2009), What controls interplate coupling?: Evidence for abrupt change in coupling across a border between two overlying plates in the NE Japan subduction zone, *Earth Planet. Sci. Lett.*, *283*, 111–121, doi:10.1016/j.epsl.2009.04.003.
- Wald, D. J., and P. G. Somerville (1995), Variable-slip rupture model of the great 1923 Kanto, Japan earthquake: Geodetic and body-waveform analysis, *Bull. Seismol. Soc. Am.*, *85*, 159–177.
- Wang, K., I. Wada, and Y. Ishikawa (2004), Stress in the subducting slab beneath southwest Japan and relation with plate geometry, tectonic forces, slab dehydration, and damaging earthquakes, *J. Geophys. Res.*, *109*, B08304, doi:10.1029/2003JB002888.
- Wessel, P., and W. H. F. Smith (1998), New, improved version of the Generic Mapping Tools released, *Eos Trans. AGU*, *79*(47), 579, doi:10.1029/98EO00426.
- Wu, F., D. Okaya, H. Sato, and N. Hirata (2007), Interaction between two subducting plates under Tokyo and its possible effects on seismic hazards, *Geophys. Res. Lett.*, *34*, L18301, doi:10.1029/2007GL030763.

---

A. Hasegawa and J. Nakajima, Research Center for Prediction of Earthquakes and Volcanic Eruptions, Graduate School of Science, Tohoku University, Aramaki-Aza-Aoba, Aoba-ku, Sendai, Miyagi 980-8578, Japan. (nakajima@aob.gp.tohoku.ac.jp)

F. Hirose, Seismology and Volcanology Research Department, Meteorological Research Institute, 1-1 Nagamine, Tsukuba, Ibaraki 305-0052, Japan.